nature energy

Article

https://doi.org/10.1038/s41560-025-01887-6

Metrics for evaluating safe electrolytes in energy-dense lithium batteries

Received: 26 May 2025

Accepted: 18 September 2025

Published online: 30 October 2025

Check for updates

Chao-Yang Wang [1] ✉, Kaiqiang Qin[1], Shanhai Ge[1], Nitesh Gupta[1], Tatsuro Sasaki[2] & Koichiro Aotani[2]

Lithium-ion batteries can fail catastrophically through thermal runaway, but the key trigger has remained unclear. Here we show that the most harmful cause is lithium oxidation reaction (LOR). This makes two types of high-energy-density battery surprisingly most dangerous: all-solid-state batteries with cracked solid separators, whether from manufacturing defects, high-pressure assembly or electrochemical cycling, and batteries with non-flammable liquid electrolytes. In both batteries, oxygen evolved from an oxide cathode passes directly to an anode, triggering highly energetic LOR. In contrast, traditional carbonate- and ether-based electrolytes are safer because they can consume O_2 in transit, alleviating or avoiding LOR. These findings apply to both lithium metal and lithiated anodes such as graphite. Safe electrolytes are thus either solid ion conductors that stop O_2 crossover under all conditions or materials that scavenge O_2 through low-exothermic reactions.

The future of all-solid-state batteries (ASSBs) for electrochemical energy storage hinges upon two pillars: high energy density and high safety[1–5]. The former necessitates using lithium metal or high-capacity lithiated anodes such as silicon. The latter is taken for granted as thermal runaway (TR) in today's lithium-ion batteries (LIBs) is blamed on flammable liquid electrolytes. It is thus assumed that ASSBs, where non-combustible solid electrolytes replace flammable liquid electrolytes, inherently provide safety guarantees. Among the touted advantages of ASSBs, safety is far more important than high energy density, because without it, lithium metal batteries would risk repeating the failed commercialization attempts by Moli Energy in the late 1980s[6].

Presently, the safety of lithium batteries is the most critical challenge for transportation electrification and renewable energy storage. TR and fires caused by overheating or short circuiting have been studied by differential scanning calorimetry, accelerated rate calorimetry and nail penetration. General discussions of battery safety abound in the literature[7–10]. Unfortunately, the literature is plagued by a lack of either quantitative reproducibility or practically meaningful experimental conditions, making it difficult to probe the fundamental science of battery TR. For example, Song et al.[11] performed nail penetration tests on six identical cells but obtained varying results, from completely safe to totally burnt. Furthermore, differential scanning calorimetry and accelerated rate calorimetry techniques are routinely applied to characterize the thermal stability of all-solid-state cells without applied pressure, whereas the cell performance and cycling tests invariably involve compression of tens of MPa (refs. 12–14).

Better safety of ASSBs is assumed based on the notion that non-combustible solid electrolytes substitute flammable liquid electrolytes, reducing the fuel available to trigger TR and fires. Most recently, the assumed safety intrinsic to ASSBs began to be seriously questioned, starting from much higher adiabatic temperatures upon TR as calculated first by Longchamps et al.[9] and later verified by Bates et al.[15] Further, Ge et al.[16] discovered that solid cells with a porous separator catch fires within 1–3 seconds upon internal shorting via lithium oxidation reaction (LOR) when oxygen evolved from an oxide cathode contacts the lithium anode through the separator. TR in solid cells with cracked separators was found to be much more rapid and violent than in cells with flammable liquid electrolytes.

In this work, we conduct single-layer internal shorting experiments in a multilayer battery, based on the recently developed resistance-controlled internal short-circuit (RISC) method[16,17]. We provide a comprehensive analysis of TR pathways, underlying mechanisms

[1]Electrochemical Engine Center (ECEC) and Department of Mechanical Engineering, The Pennsylvania State University, University Park, PA, USA. [2]Nissan Research Center, Nissan Motor Co. Ltd, Yokosuka, Japan. ✉e-mail: cxw31@psu.edu

https://doi.org/10.1038/s41560-025-01887-6

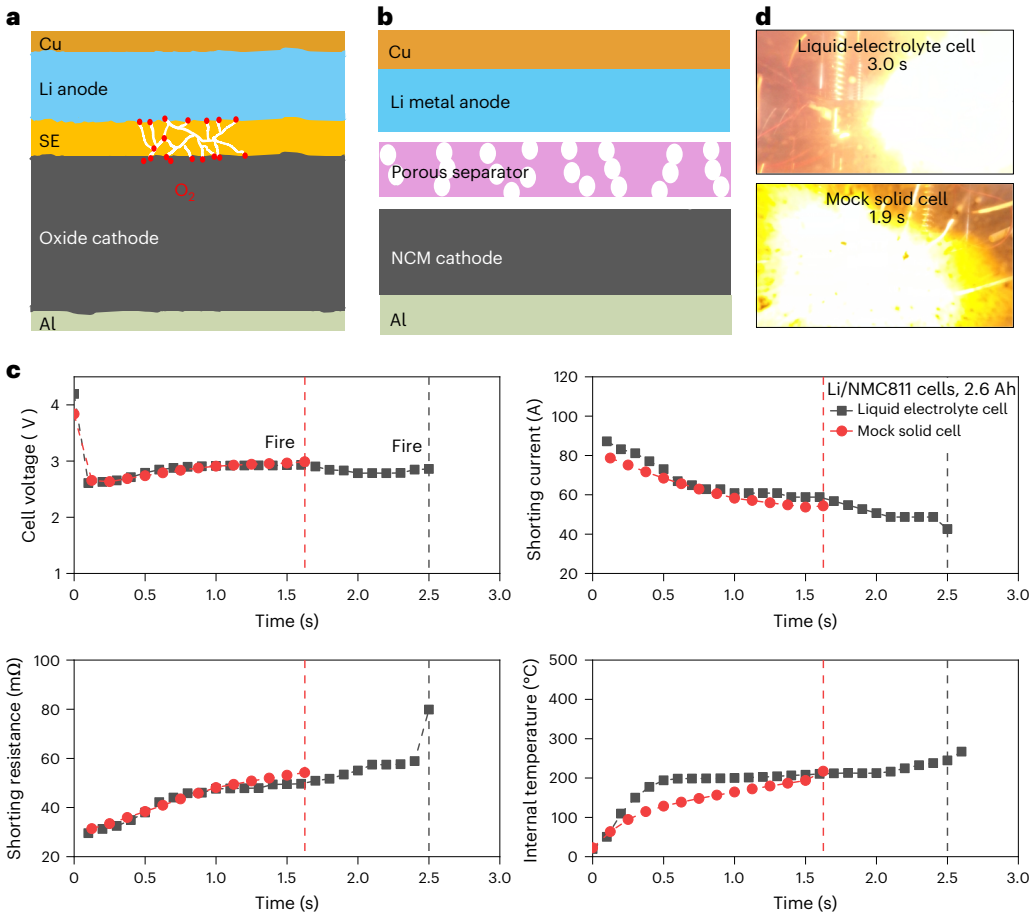

Fig. 1 | Single-layer ISC of lithium batteries. a, Schematic illustration of lithium oxidation reaction in an all-solid-state cell with cracked solid separator. **b**, A mock solid cell where a porous separator simulates a cracked solid separator. **c**, Temporal variations of voltage, shorting current, shorting resistance and internal temperature of the liquid electrolyte cell versus the mock solid cell upon ISC. The vertical dashed lines denote the onset of fire. **d**, Photographic images of the liquid electrolyte cell and the mock solid cell catching fire after ISC.

and energetics, challenging the conventional wisdom that ASSBs are intrinsically safe. Our findings reveal that upon internal shorting, solid cells with cracked separators or cells with non-flammable liquid electrolytes are more dangerous than conventional cells with flammable liquid electrolytes. Finally, we offer insights into designing safe electrolytes for high-energy-density lithium batteries.

Most harmful lithium oxidation for thermal runaway

In a high-energy-density ASSB, a lithium metal anode is paired to a high-capacity layered oxide cathode such as $LiNi_{0.8}Co_{0.1}Mn_{0.1}O_2$ (NCM811) with a solid separator sandwiched in between. Should the solid separator crack or break, LOR becomes possible (Fig. 1a):

$$4Li + O_2 \rightarrow 2Li_2O \qquad \Delta H = 4.3 \times 10^7\,J\,kg^{-1} \text{ or } \sim 12,000\,Wh\,kg^{-1} \tag{1}$$

where ΔH is the heat of combustion. This reaction is most violent and energetic in lithium batteries, and it requires an oxygen-fuel molar ratio of only 0.25, whereas a delithiated NCM cathode can theoretically release 0.5 oxygen per fuel. Thus, there is sufficient oxygen supply from layered oxide cathodes even if a battery cell remains a closed space. Ge et al.[16] described several high-probability scenarios where a solid separator fails and lithium metal and O_2 come in contact, whether arising from defective manufacturing of solid separators, mechanical stress due to high-pressure cell assembly or usage. One such example is the connected cracks formed across a ceramic separator after repetitive charge–discharge cycles, as demonstrated by the Bruce group[18].

In this work we created a mock solid cell to simulate a generic ASSB with a cracked solid separator like the one shown by the Bruce group[18]. As schematically sketched in Fig. 1b, the mock cell starts with a standard anode-free battery (AFB) with one layer of NCM811 cathode, a bare Cu foil current collector and a ceramic-coated porous separator filled with a localized high-concentration electrolyte (LHCE) consisting of LiFSI salt in dimethoxyethane (DME) solvent and 1,1,2,2-tetrafluoroethyl-2,2,3,3-tetrafluoropropylether (TTE) diluent (LiFSI:DME:TTE = 1:1.2:3 by molar). The cell undergoes formation and is charged to deposit a lithium anode in situ. Then, the cell is open in a glovebox to inject 10 ml DME. After standing for 3 hours, the DME is removed. Such a rinsing process is repeated twice to thoroughly remove all electrolyte. The washed cell is then placed in a glovebox for vacuum drying overnight at 25 °C and subsequently resealed to create a liquid-free cell with a porous separator to simulate a cracked solid separator. Such a mock solid cell is then placed in the RISC test apparatus as schematically illustrated in Extended Data Fig. 1. Two thin metal chips embedded in the single-layer test cell and connected externally by a shunt and a switch are used to induce internal shorting with precisely controlled shorting resistance, thereby ensuring high reproducibility[16,17]. A thermocouple placed at the centre of the separator in the shorting area monitors the internal temperature. An external power source simulating neighbouring un-shorted layers in a multilayer battery is connected in parallel with the single-layer test cell to be shorted. Physically, the experimental set-up replicates the

https://doi.org/10.1038/s41560-025-01887-6

Table 1 | Heat of combustion per cm^2 of electrodes in various batteries

	Fuel sources		Reactions	Fuel mass (kg cm^{-2})	O_2 consumption (kg cm^{-2})	Heat of combustion (J kg^{-1})	Theoretical heat (J cm^{-2})	Percent of reaction based on O_2 available	Heat (J cm^{-2})
LIBs with Gr anode	Liquid electrolyte	EC (30 wt%)	$C_3H_4O_3+2.5O_2=3CO_2+2H_2O$	1.70E−06	1.54E−06	1.21E+07 (ref. 25)	20.57	29%	27.1
		EMC (70 wt%)	$C_4H_8O_3+4.5O_2=4CO_2+4H_2O$	3.96E−06	5.48E−06	1.84E+07 (ref. 26)	72.86		
		LiC_6	$LiC_6+0.25O_2=0.5Li_2O+C_6$	10.02E−06	1.02E−06	3.56E+06 (ref. 27)	35.67	0%	0
		Total heat*							**27.1**
	ASSB	LiC_6	$LiC_6+0.25O_2=0.5Li_2O+C_6$	10.02E−06	1.02E−06	3.56E+06 (ref. 27)	35.67	100%	35.7
		Total heat							**35.7**
AFBs	Liquid electrolyte	DME	$C_4H_{10}O_2+5.5O_2=4CO_2+5H_2O$	1.12E−06	2.18E−06	3.17E+07 (ref. 28)	35.50	36%	39.9
		TTE	$C_5H_4F_8O+3.5O_2=4HF+CF_4+4CO_2$	7.19E−06	3.47E−06	1.05E+07**	75.50		
		16.5 µm Li deposited at 100% SOC	$Li+0.25O_2=0.5Li_2O$	0.88E−06	1.02E−06	4.30E+07 (ref. 27)	37.84	0%	0
		Total heat							**39.9**
	ASSB	16.5 µm Li deposited at 100% SOC	$Li+0.25O_2=0.5Li_2O$	0.88E−06	1.02E−06	4.30E+07 (ref. 27)	37.84	100%	37.8
		Total heat							**37.7**
ASSBs with 20 µm Li foil	20 µm Li foil+16.5 µm Li deposited		$Li+0.25O_2=0.5Li_2O$	1.95E−06	2.25E−06	4.30E+07 (ref. 27)	83.85	90%	75.7
	Total heat								**75.7**

*Total heat denotes the summation of all heats generated in a cell. Other acronyms include EC, ethylene carbonate; EMC, ethyl methyl carbonate; LiC_6, lithiated graphite; and SOC, state of charge. **A. C. T. Van Duin, personal communication. The calculation is based on a 3.4 mAh cm^{-2} cathode loading and a maximum of 2.03×10^{-6} kg cm^{-2} O_2 releasable from NCM811 cathodes. The columns of fuel mass, O_2 consumption, heat of combustion, theoretical heat, percent of reaction based on O_2 available and heat represent the mass loading of a fuel, stoichiometric consumption of O_2 per the amount of fuel, thermodynamic heat of complete fuel combustion, theoretical heat of the complete fuel combustion, percent of the complete fuel oxidation based on available O_2 and actual heat generated with both fuel and O_2 available (that is, multiplying the columns of theoretical heat with percent of reaction based on O_2 available), respectively. Bold fonts highlight the total heat of all reactions.

most severe failure scenario, that is, internal short circuiting (ISC) of a single layer in a multilayer battery. More details and discussions on the RISC method can be found in ref. 16.

Figure 1c compares the internal shorting of a mock solid cell with a LHCE-filled counterpart with respect to cell voltage, shorting current, shorting resistance and internal temperature as functions of time. The mock solid cell is seen to catch fire at 1.6 s (marked by the vertical dashed line in Fig. 1c), even earlier than 2.5 s of the liquid LHCE cell. This can be explained by the facile transport of oxygen gas released from the NCM cathode into the lithium metal anode through open pores of the separator and subsequent triggering of LOR according to equation (1). Pictures of the mock solid cell and liquid electrolyte cell after ISC testing can be seen from Supplementary Fig. 1. High potency of fires and TR in ASSBs can be further inferred from Fig. 1c where fire breaks out at an internal temperature of only ~200 °C in the mock solid cell, whereas it takes ~300 °C for the fire onset in the liquid cell. Other ISC quantities, such as cell voltage, shorting current and shorting resistance, remain almost the same between the two cells, as shown in Fig. 1c. Figure 1d displays fire images of the mock solid cell and liquid cell, respectively.

It is striking that TR and fires in solid cells ignited by LOR can occur at rather low temperatures (~ 200 °C). While theoretically, the product of LOR, that is, Li_2O, forms a passivation layer[19], lithium metal becomes liquid under the ISC conditions as it has a low melting point (180 °C). Lithium melting renders the passivation layer Li_2O practically useless. This fact implies that protective surface coatings on Li metal are probably futile under abuse.

Table 1 tabulates the thermodynamic heat of combustion occurring in three types of battery, LIBs with graphite anodes, anode-free AFBs and ASSBs with 20-µm Li foils. All have the same NCM811 cathode of 3.4 mAh cm^{-2} and hence an equal maximum releasable oxygen. Both LIB and AFB types further have solid and liquid electrolyte versions, respectively. It is seen that in the LIB category, liquid electrolytes can reduce quite a bit of oxygen and only 29% of organic solvents needs to be oxidized by cathode-releasing O_2 to yield limited heat. Interestingly, this combustion of 29% organic solvents effectively protects the triggering of much more energetic LOR in the lithiated graphite by depleting oxygen. Indeed, if a solid electrolyte replaces the liquid in a current LIB, oxygen released from the NCM cathode will fully pass through and react with the lithiated graphite anode in case of a cracked separator, generating 32% more heat. Further, if an ASSB is built with 20-µm Li foil as the anode as in prevalent ASSBs of high energy density, the combustion heat to cause TR and fires becomes 75.7 versus 27.1 J cm^{-2} in a LIB. This is a 280% jump in heat generation, making ASSBs much more dangerous than liquid electrolyte LIBs thermodynamically. Fundamentally, it is noted in Table 1 that combustion heat release in lithium batteries is controlled by O_2 availability, with LOR having 1,190 kJ mol^{-1} O_2 versus liquid electrolyte combustion of 470 kJ mol^{-1} O_2. Thus, LOR must be avoided or suppressed by all means in lithium batteries, including ASSBs.

A common view about safety improvement of ASSBs is attributed to the substitution of flammable liquid electrolytes by solid electrolytes and hence less fuel amount contained. This view proves incorrect per Table 1 showing that the combustion heat is controlled by O_2 availability, not the fuel amount, when solid or liquid cells are still sealed systems. The same amount of O_2 released from the oxide cathode produces reaction heat of 1,190 kJ mol^{-1} O_2 through LOR in ASSBs while

https://doi.org/10.1038/s41560-025-01887-6

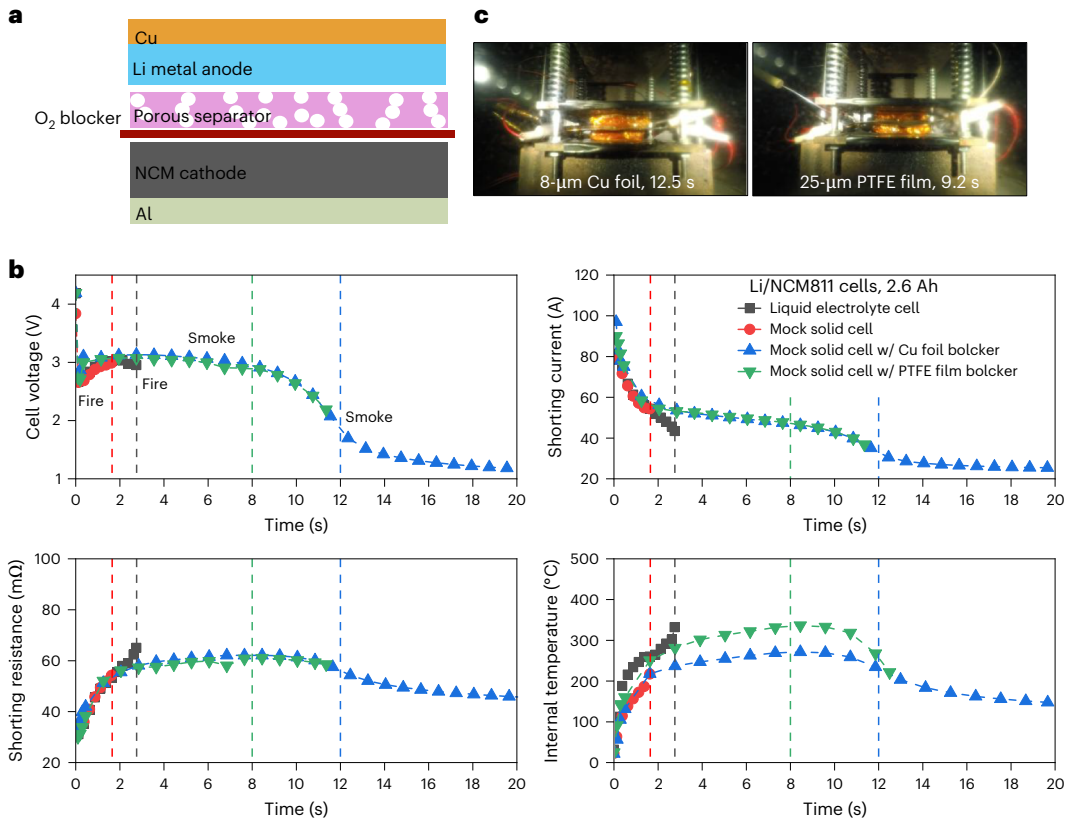

Fig. 2 | Internal short circuiting of solid cells with oxygen crosstalk blocked. **a**, Schematic illustration of a mock solid cell with an O_2 blocker inserted between the cathode and separator. **b**, Smoking of solid cells with 8-μm Cu foil and 25-μm PTFE film as O_2 blocker upon ISC versus catching fire of the solid cell without O_2 blocker and the liquid electrolyte cell. **c**, Photos of the solid cells with Cu foil and PTFE film as O_2 blockers, respectively, after ISC, showing smokes only. The verticle dashed lines denote the onset of fire or smoke.

it generates only ~470 kJ mol^{-1} O_2 through the combustion of organic electrolytes in liquid cells. When comparing a liquid electrolyte LIB with a solid electrolyte LIB listed in Table 1, the total fuel amount is indeed much more in the liquid case (LiC_6 plus the organic solvents totalling 129.1 J cm^{-2}) than the solid cell (LiC_6 of 35.7 J cm^{-2}); however, the actual combustion heat generated based on the available O_2 is still higher in the solid cell (35.7 J cm^{-2}) than the liquid cell (27.1 J cm^{-2}), due primarily to much higher utilization of O_2 in LOR to generate heat. Furthermore, if one compares a standard ASSB with 20-μm Li foil anode with a liquid LIB, the difference in the total fuel diminishes, with 83.85 J cm^{-2} in the ASSB versus 129.1 J cm^{-2} in the LIB, but combustion heat generated based on O_2 availability is 75.7 J cm^{-2} for the ASSB, in contrast to only 27.1 J cm^{-2} for the liquid LIB. This huge jump in combustion heat in a common ASSB, as compared to a standard liquid electrolyte LIB, strongly suggests that ASSBs are much more hazardous than commercially available LIBs under abuse.

To further test the hypothesis that LOR holds the key to the safety of lithium batteries, we devised several mock solid cells with oxygen blockers (that is, a 25-μm polytetrafluoroethylene (PTFE) solid film and an 8-μm Cu foil) inserted between the NCM cathode and separator, as shown in Fig. 2a. The goal is to completely block the crosstalk between cathode oxygen and anode lithium. Internal shorting of such cells with O_2 blockers indeed shows that fires vanish with only slight smoke, probably generated from the burning of binders and carbon fillers in the NCM cathode due to ISC-created localized heating. This is in stark contrast to the mock solid cell and liquid LHCE cell catching fires at 1.6 and 2.5 s, respectively (Fig. 2a). Further, the 8-μm Cu foil blocker cell is seen to exhibit a lower temperature at the shorting spot than 25-μm PTFE film, implying that both properties of O_2 barrier and high thermal mass are helpful to suppress fire formation. The experimental cells with O_2 blockers were opened for electrode examination after ISC testing. As shown in Supplementary Fig. 2, the cathode in the red dashed areas and the corresponding separator exhibited an obvious colour difference compared to the other areas, indicating that the light smoke resulted from the partial burning of the cathode binder and separator.

The importance of oxygen availability to cause LOR was also addressed in Ge et al.[16] via lithium iron phosphate (LFP) cathodes and low-SOC NCM811 cathodes where the former does not release oxygen while the latter produces less oxygen. Both cases led to no fire. Note however that making an ASSB cell with LFP may be less appealing for practical applications due to rather low energy density and already high safety of liquid electrolyte LFP batteries. A better step forward is to pursue high-capacity cathode materials that release little or no O_2 upon heating[20].

Limitations of non-flammable electrolytes

There has been a large but perplexing body of literature on safe liquid electrolytes for lithium batteries. The conventional belief is that non-flammable electrolytes reduce the fuel available for combustion and remove a main cause for TR thus leading to ultimate battery safety. However, experimental evidence remains largely controversial and inconclusive[21,22].

Here we demonstrate RISC experiments of mock solid cells refilled with an ionic liquid (Py_{13}TFSI; IL) and a high-concentration phase change electrolyte (LiFSI:Sulfolane:DME = 2.1:0.8:0.4 by molar; HPCE), respectively, after the test cells undergo formation and in situ deposition of lithium anode by the LHCE electrolyte and then are rinsed by DME and vacuum dried to remove the LHCE electrolyte. The IL is completely non-flammable, whereas the HPCE containing a large amount of sulfolane has low volatility but is combustible with a large

https://doi.org/10.1038/s41560-025-01887-6

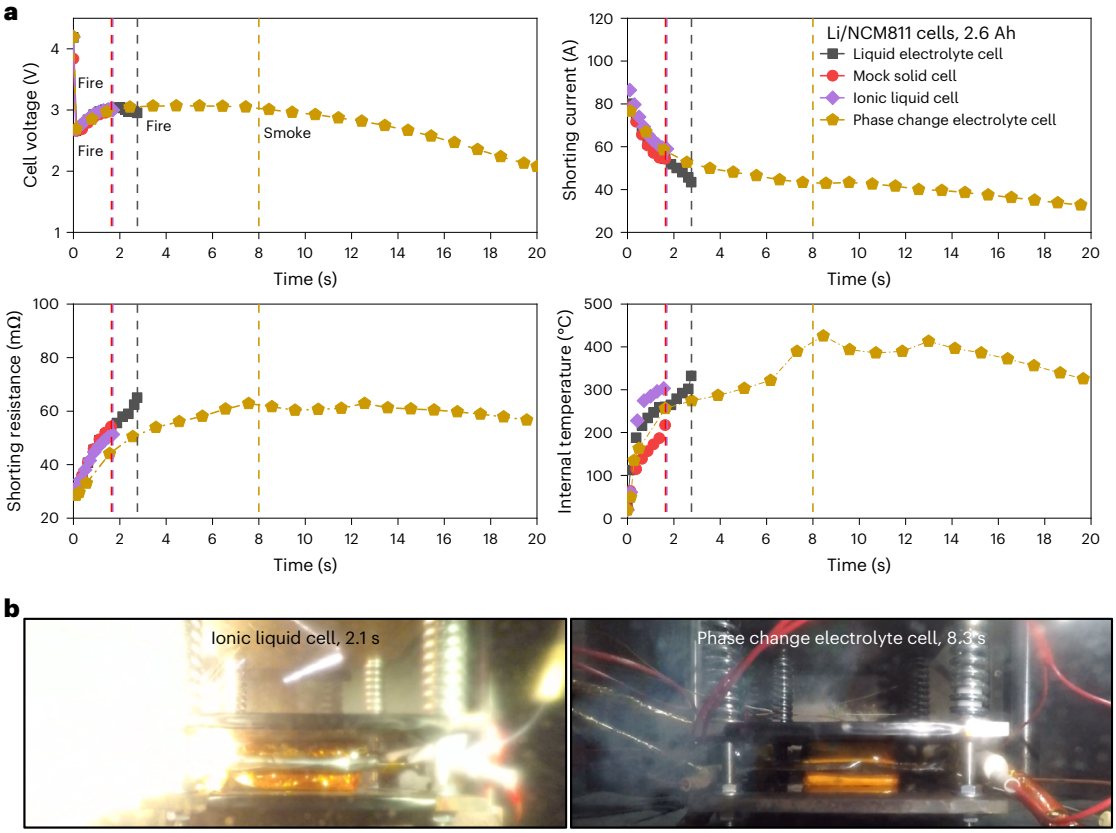

Fig. 3 | Internal short circuiting of anode-free batteries filled with an IL and a HPCE. a, IL cell catches fire as rapidly as the mock solid cell and faster than the LHCE liquid electrolyte cell, whereas the less volatile HPCE cell emits smoke only. **b**, Photos of the IL and HPCE cells after ISC, with the IL cell catching violent fire but the HPCE cell smoking heavily. The verticle dashed lines denote the onset of fire or smoke.

oxygen reduction capacity. Surprisingly, it is seen in Fig. 3a that the IL cell catches fire after 1.7 s, almost identical to the mock solid cell with an open, dry separator. This is because O_2 evolved from the NCM cathode bubbles straight to the lithium metal anode through the ionic liquid without being reduced, thereby triggering the violent and energetic LOR for TR and fires. Pictures of the IL cell after ISC testing are shown in Supplementary Fig. 3.

These experiments suggest that all non-flammable electrolytes, including ionic liquids and cracking solid electrolytes, do not result in better safety. In contrast, the HPCE cell containing a large amount of sulfolane to reduce cathode-released O_2 does not catch fire but emits smoke after approximately 8 s, causing very mild TR (Fig. 3b and Supplementary Fig. 4). Sulfolane oxidation yields ~470 kJ mol^{-1} O_2 as compared to 1,190 kJ mol^{-1} O_2 of LOR, so it is much more benign than LOR. The sharp contrast in ISC consequences between a non-flammable ionic liquid and a combustible HPCE electrolyte, shown in Fig. 3a,b, is revealing.

We chose an IL for demonstration because it represents the most non-flammable extreme of all liquid electrolytes, including phosphorus- and fluorine-based electrolytes, their mixtures, high-concentration electrolytes and ILs-based electrolytes. When a liquid electrolyte does not have the oxygen reduction capacity, the cell will trigger the most energetic and violent LOR as oxygen evolved from an oxide cathode upon abuse must fully cross over to the lithium anode. Thus, the experiments presented here strongly suggest that non-flammable electrolytes lacking oxygen reduction capacity are more dangerous than organic electrolytes that can reduce oxygen partially or fully.

Fire risks of LIB cells with lithiated anodes

Another interesting question is whether battery safety can be dramatically improved if lithium metal is replaced by a lithiated anode such as graphite or silicon. Thermodynamically, oxidation of lithiated anodes such as LiC_6 and $Li_{22}Si_5$ yields the same combustion heat per unit of Li mass. In lithium batteries, the lithium mass loading is determined by the cathode capacity and a narrow-ranging negative-to-positive capacity ratio; hence, it is almost irrespective of the anode type. Thus, it can be expected that a mock solid cell described above, but substituted with a lithiated anode such as LiC_6, will catch fire upon internal shorting, although the resulting TR fires could be damped somewhat owing to the additional large thermal mass of host materials (for example, graphite). To test such a hypothesis, we built mock solid cells with graphite anodes instead of bare Cu foils. We tested them in the RISC set-up for two cell capacities of 5 and 9.5 Ah (that is, the external power sources), respectively. These solid cells are further contrasted to liquid electrolyte LIB cells filled with a standard electrolyte (1.2 M $LiPF_6$ in EC:EMC = 3:7 by weight) at the same cell capacities. It is seen from Fig. 4a that at both large and small capacities, solid LIB cells catch fire at 1.6 s and 1.8 s upon internal shorting, respectively. Pictures of the burned cells and their electrodes after ISC testing are shown in Supplementary Figs. 5 and 6. Comparing Fig. 1c (solid AFB cell, 2.6 Ah) with Fig. 4a (solid LIB cell, 5 Ah), it is noted that the graphite host in the LIB cell anode pushes the threshold cell capacity for fire formation higher (from 2.6 to 5 Ah) and delays the ignition temperature from ~200 to ~300 °C. Nevertheless, this improvement in safety is achieved at the expense of energy density, as the LIBs exhibit lower energy density compared to the AFBs.

On the other hand, the liquid LIB cell only emits smoke when the cell capacity is 5 Ah and starts to catch fire when the cell capacity increases to 9.5 Ah (Supplementary Figs. 7 and 8). Figure 4b displays images of battery fires after the pouch bags break for liquid and solid cells under 5 Ah, respectively, showing that at 5 Ah, the solid LIB cell with graphite anode without any flammable liquid electrolyte can catch fire upon internal shorting, whereas the liquid LIB cell does not. Again,

https://doi.org/10.1038/s41560-025-01887-6

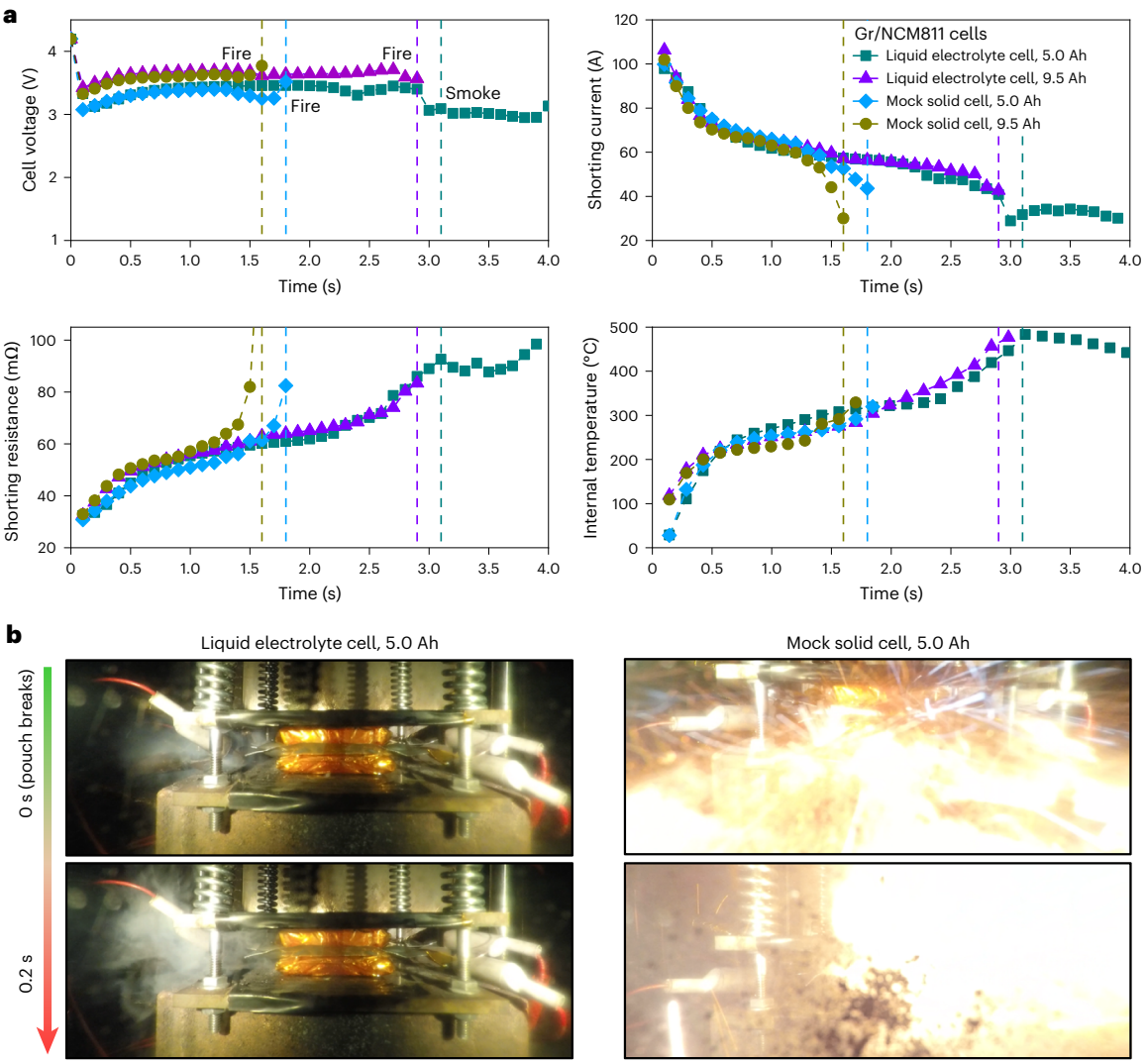

Fig. 4 | Internal short circuiting of graphite||NCM811 LIBs. a, Temporal variations of voltage, shorting current, shorting resistance and internal temperature of the liquid electrolyte cell versus the mock solid cell upon ISC, at cell capacities of 5 and 9.5 Ah, respectively. Both liquid and solid cells catch fire at 9.5 Ah, but at 5 Ah, the mock solid cell catches fire whereas the liquid cell smokes only. **b**, Photographic images of the liquid and mock solid cells at 5 Ah after ISC. The verticle dashed lines denote the onset of fire or smoke.

this demonstrates that solid cells with cracked separators are more dangerous than liquid cells, even with graphite anodes, in accordance with the thermodynamic calculations of actual combustion heat based on O_2 availability shown in Table 1. Here we experimentally prove that the cause of TR in commercially available LIBs is not flammable liquid electrolytes. Rather, one should avoid triggering the most violent and energetic LOR when oxygen evolved from an oxide cathode comes in contact with a lithiated anode.

Insights into safe electrolytes

The vast literature has qualitatively described safe electrolytes as having good electrochemical stability, high thermal stability, non-flammability and low volatility. Critically, organic electrolytes, whether carbonate- or ether-based, are widely blamed as a major cause of battery TR[7,10,21]. If we define the main cause as something without which TR will not occur, then our experiments with liquid-free cells experiencing violent TR demonstrate that organic liquid electrolytes are clearly not the cause of TR. There has been much debate on non-flammable electrolytes for battery safety in the literature[22,23]. The experiments presented here again unambiguously show that ionic liquids, the idol of non-flammable liquid electrolytes, are more dangerous than organic electrolytes in causing TR and fires.

To seek a definitive and quantitative guideline for safe electrolytes that will not cause TR, we create a new plot of the mass-specific reaction heat in kJ g^{-1} versus the O_2 reduction capacity in mol O_2 g^{-1} for combustible reactants commonly present in lithium batteries as shown in Fig. 5. As expected, it is seen that lithiated graphite LiC_6, lithiated silicon $Li_{22}Si_5$ and lithium metal all fall on a linear line with the same slope of 1,190 kJ mol^{-1} O_2, characteristic of LOR. Interestingly, most organic solvents such as DME, EC, EMC, SF and TTE can be fitted in another straight line with a slope of ~470 kJ mol^{-1} O_2. The larger the line slope is in Fig. 5, the more energetic the reaction to cause TR. Thus clearly, if oxidation of lithiated anodes is provoked and triggered, the most dangerous TR ensues. On the other hand, if the combustion of organic liquid electrolytes occurs to divert and avoid LOR, there would be better battery safety. Also included in Fig. 5 are carbon and iron. It is noteworthy that carbon is a better O_2 scavenger than most organic solvents, yielding less heat. Being the most common O_2 scavenger in food packaging applications, Fe is seen to have similar heat release to the most dangerous LOR governing oxidation of lithiated anode materials. Finally, there are materials that can scavenge O_2 through endothermic reactions, such as halide solid electrolyte Li_3InCl_6 (ref. 24), also shown in Fig. 5. Unfortunately, Li_3InCl_6 has a tiny O_2-scavenging

https://doi.org/10.1038/s41560-025-01887-6

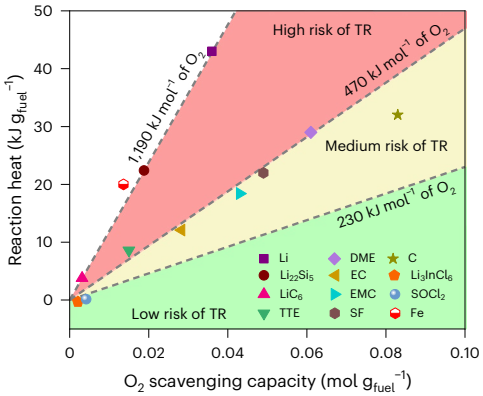

Fig. 5 | Metrics of safe electrolytes for lithium batteries. Electrolytes without oxygen reduction capability, such as cracked solid electrolytes and ionic liquids, cause the most energetic LOR in lithium metal or lithiated anodes and hence are high risk for TR. Flammable liquid electrolytes yield medium combustion heat and represent medium risk for TR. Safe electrolytes should have high O_2-scavenging capacity but yield reaction heat lower than 230 kJ mol^{-1} O_2. Additional data of sulfolane (SF), carbon (C), $SOCl_2$ and iron (Fe) are taken from refs. 29–32.

capacity and hence would require a massive mass to reduce O_2 released from battery cathodes.

We estimate that electrolytes or additives with a slope less than 230 kJ mol^{-1} O_2 are preferably needed for intrinsic safety, as sketched in Fig. 5. As an illustrative example, thionyl chloride $SOCl_2$ is shown in Fig. 5 to have a slope of only 32 kJ mol^{-1} O_2 and an O_2-scavenging capacity of 0.0084 mol O_2 g^{-1} although the latter property is too small to make $SOCl_2$ useful. Approximate estimate of the half slope for safe electrolytes is based on the idea that 50%-SOC cells with liquid electrolytes of 470 kJ mol^{-1} O_2 were found to incur neither fire nor smoke in lithium metal cells by Ge et al.[16] (Fig. 4b therein), due to producing only half of reaction heat from electrolyte oxidation. This is further confirmed in Gr/NCM811 LIBs as shown in Extended Data Fig. 2. Thus, we posit that in 100%-SOC cells, if we could cut down the electrolyte oxidation heat to half through slashing the slope to 230 kJ mol^{-1} O_2, there would be a good chance to suppress fire formation. Future work is needed to establish the safe slope more quantitatively.

The present work suggests that there may be two potential routes to develop safe electrolytes for lithium batteries of high energy density. One is to develop defect-free solid separators that retain absolute impermeability to oxygen under any conditions. This may be a very tall order as the impermeability requirement must be met uniformly over a large footprint area of separators employed in a large-format EV battery, withstand extremely high stacking pressures up to tens of MPa and survive through long-term cycling and storage. The second route is to develop O_2-scavenging electrolytes or additives that are highly efficient in consuming oxygen through a low-exothermic (for example <230 kJ mol^{-1} O_2) or preferably endothermic reaction. Work is ongoing in this direction.

Conclusions

We show that the leading cause for battery TR and fires is the highly energetic LOR occurring at low temperatures of 200–300 °C and in the timescale of a few seconds. Electrolytes that cannot stop the crossover of oxygen from cathode to anode or reduce oxygen to prevent LOR are more prone to TR. This includes solid electrolytes with cracked separators and non-flammable liquid electrolytes. Developing O_2-scavenging electrolytes is paramount for improving battery safety. Additionally, high-capacity cathode materials that release little or no O_2 upon heating also offer promise for safer energy-dense batteries. Protective surface coating of lithium anode materials, however, may be ineffective considering that lithium metal becomes shapeless liquid at its low melting point of 180 °C. Work is underway to control LOR and make ASSBs safe, even in the presence of cracked solid separators.

Methods

Cell materials and fabrication

We fabricated 0.15-Ah single-layer AFBs using $LiNi_{0.8}Co_{0.1}Mn_{0.1}O_2$ (NCM811) cathodes of 16.51 mg cm^{-2} and 8-µm copper foil for the anode current collector. The design details are listed in Supplementary Table 1. Each AFB cell consists of two copper current collectors and one double-side coated cathode layer with a 25-µm thick ceramic-coated separator (Lucky) in between. Inside each experimental cell designed for ISC measurements, we placed two thin chips (4 × 4 mm, 100-µm thick) made of either aluminium or nickel, as shown schematically in Extended Data Fig. 1. These chips are wired to the outside and connected to a switch and a shunt for current sensing. The cathode portion underneath the aluminium chip is peeled off, allowing direct contact between the chip and the aluminium current collector. The anode and cathode have dimensions of 44 × 56 and 42 × 54 mm, respectively. The electrolyte was prepared in an Ar-filled MBraun glovebox with both water and oxygen levels of <0.1 ppm. Each cell was filled with 0.45 g of electrolyte and packaged in Al-laminated pouch bags of 113 µm in thickness. For the preparation of mock solid AFB cells, the AFB cells filled with LHCE were opened in glovebox after the formation process and rinsed by DME to completely remove LHCE. After vacuum drying overnight, the mock solid AFB cells were resealed.

LIB cells are built by using the same NCM811 cathodes as in the lithium metal cells and artificial graphite anodes with the negative-to-positive capacity ratio of 1.1. Both the NCM cathode and Gr anode portion underneath the chips are peeled off, allowing direct contact between the chips and the current collectors. Each Gr/NCM cell consists of one double-sided coated Gr anode and two double-sided coated NCM cathode layers with a 25-µm thick ceramic-coated separator (Lucky) in between. These cells were refilled with 1.2 M $LiPF_6$ in EC:EMC = 3:7 (by weight) electrolyte with all other materials remaining the same. For the preparation of mock solid Gr/NCM cells, the Gr/NCM cells filled with liquid electrolyte were opened in glovebox after the formation process and rinsed by EMC to completely remove liquid electrolyte. After vacuum drying overnight, the mock solid Gr/NCM cells were resealed.

Resistance-controlled internal short circuit method

All cells were initially cycled at 25 °C and C/10 for one cycle, followed by charging to 100% SOC. During the formation and subsequent RISC testing, a pressure of 0.35 MPa was always applied to each experimental cell, which is placed in a cell holder shown in Extended Data Fig. 1. The test cell is sandwiched between two ceramic blocks of 10 mm in thickness for thermal insulation between the test cell and pressure clamping components. A load cell in the holder is used to indicate the applied cell pressure. It was found that a pressure between 0.35 and 1.2 MPa is needed to generate reproducible and consistent shorting resistance and, hence, ISC tests, as the contact resistance between various layers of the cell drops to within 3% of the total shorting resistance in this clamping pressure range. In addition, the shorting resistance may be varied by selecting different shorting chip materials and sizes to simulate a range of short-circuit scenarios.

Each experimental cell has two shorting-measurement terminals and two regular anode and cathode terminals connected in parallel to a large-format Li-ion cell serving as an external energy source (such as 2.6 Ah, 5.0 Ah and 9.5 Ah), as shown in Supplementary Fig. 9. Once the switch between the two shorting terminals is closed, an equivalent anode–cathode ISC is triggered, with simultaneous measurement of ISC current. The energy source supplies a large shorting current to rapidly heat the experimental single-layer cell. The resistance between the two measurement chips and their corresponding tabs is measured by the voltage drop across these two terminals.

Thin thermocouples were embedded in the cell or attached to its outer surface to monitor the temperatures during ISC and subsequent stages. In this experimental system, the capacity of the experimental single-layer cell is negligibly inconsequential because the majority of the shorting current is provided by the external power source. This allows for testing across a wide range of scenarios, including different cell chemistry and materials such as lithium metal versus graphite anodes and liquid versus solid electrolytes.

With both shorting current I_s and resistance R_s measured, the ohmic heat generation rate at the ISC location can be estimated by $I_s^2R_s$. We use one shunt connected to the chip terminals to measure the total shorting current and another shunt in the circuit to measure the current output of the external power source. Both switches for single-layer cell shorting and external power source are activated simultaneously (Extended Data Fig. 1 and Supplementary Fig. 9). The ISC cell was put in a steel chamber with a ventilation system. A GoPro camera (HERO12) was put outside of the chamber to record the whole ISC process through a glass window.

Morphological and compositional characterization of anodes

Supplementary Fig. 10 shows scanning electron microscope images and X-ray photoelectron spectroscopy (XPS) spectra of the fresh deposited Li on Cu foil of the LHCE cell at 25 °C after formation. The fresh Li metal anode in the AFB cell using LHCE as electrolyte shows dense and chunk structure with a thickness of around ~24.3 µm. The solid electrolyte interphase layer constructed on Li metal anode of the LHCE cell shows the inorganic species-enriched structure contains LiF, Li_2O and Li_2CO_3. Supplementary Fig. 11 shows scanning electron microscope images and XPS spectra of the fresh deposited Li on Cu foil of the high-concentration phase change electrolyte (HPCE) cell at 60 °C after formation. Similarly, the fresh Li metal anode in the HPCE cell also shows dense and chunk structure with a thickness of around ~24.8 µm. The intense F 1*s* XPS peaks at 684.6 eV and 688 eV indicate the coexistence of LiF and organic fluoride species on the surface of Li metal in HPCE. In addition, the observation of O 1*s* XPS peaks at 528 eV and 531 eV demonstrates the formation of Li_2O and Li_2CO_3 in the solid electrolyte interphase layer in the HPCE cell at 60 °C.

Data availability

All data generated or analysed during this study are included in this published article and the Supplementary Information.

References

1. Kamaya, N., Homma, K., Yamakawa, Y., Hirayama, M. & Kanno, R. A lithium superionic conductor. *Nat. Mater.* **10**, 682–686 (2011).
2. Manthiram, A., Yu, X. & Wang, S. Lithium battery chemistries enabled by solid-state electrolytes. *Nat. Rev. Mater.* **2**, 16103 (2017).
3. Janek, J. & Zeier, W. G. Challenges in speeding up solid-state battery development. *Nat. Energy* **8**, 230–240 (2023).
4. Li, Y. et al. A lithium superionic conductor for millimeter-thick battery electrode. *Science* **381**, 50–53 (2023).
5. Wang, C. & Su, X. The promise of solid-state batteries for safe and reliable energy storage. *Engineering* **21**, 32–35 (2023).
6. Jarratt, E. New lessons from the epic story of Moli Energy, the Canadian pioneer of rechargeable lithium battery technology. *Electric Autonomy Canada* (18 September 2020).
7. Doughty, D. & Roth, E. P. A general discussion of Li ion battery safety. *Electrochem. Soc. Interface* **21**, 37–44 (2012).
8. Feng, X., Ren, D., He, X. & Ouyang, M. Mitigating thermal runaway of lithium-ion batteries. *Joule* **4**, 743–770 (2020).
9. Longchamps, R. S., Yang, X. G. & Wang, C. Y. Fundamental insights into battery thermal management and safety. *ACS Energy Lett.* **7**, 1103–1111 (2022).
10. Bates, A. et al. A multi-scale framework for advancing battery safety through early calorimetric analysis of materials and components. *Electrochem. Soc. Interface* **33**, 69–76 (2024).
11. Song, I. T. et al. Thermal runaway prevention through scalable fabrication of safety reinforced layer in practical Li-ion batteries. *Nat. Commun.* **15**, 8294 (2024).
12. Inoue, T. & Mukai, K. Are all-solid-state lithium-ion batteries really safe? Verification by differential scanning calorimetry with an all-inclusive microcell. *ACS Appl. Mater. Interfaces* **9**, 1507–1515 (2017).
13. Johnson, N. B. et al. Assessing the thermal safety of a Li metal solid-state battery material set using differential scanning calorimetry. *ACS Appl. Mater. Interfaces* **15**, 57134–57143 (2023).
14. Chen, R. et al. The thermal stability of lithium solid electrolytes with metallic lithium. *Joule* **4**, 812–821 (2020).
15. Bates, A. M. et al. Are solid-state batteries safer than lithium-ion batteries?. *Joule* **6**, 742–755 (2022).
16. Ge, S. et al. Quantification of lithium battery fires in internal short circuit. *ACS Energy Lett.* **9**, 5747–5755 (2024).
17. Qin, K., Ge, S., Gupta, N., Sasaki, T. & Wang, C. Y. High heat tolerance and safety of lithium metal batteries using a high concentration phase change electrolyte. *J. Power Sources* **630**, 236094 (2025).
18. Ning, Z. et al. Dendrite initiation and propagation in lithium metal solid-state batteries. *Nature* **618**, 287–293 (2023).
19. Kamphaus, E. P. et al. Role of inorganic surface layer on solid electrolyte interphase evolution at Li-metal anodes. *ACS Appl. Mater. Interfaces* **11**, 31467–31476 (2019).
20. Cui, Z., Liu, C., Wang, F. & Manthiram, A. Navigating thermal stability intricacies of high-nickel cathodes for high-energy lithium batteries. *Nat. Energy* **10**, 490–501 (2025).
21. Xu, K. Nonaqueous liquid electrolytes for lithium-based rechargeable batteries. *Chem. Rev.* **104**, 4303–4418 (2004).
22. Jia, H. et al. Is nonflammability of electrolyte overrated in the overall safety performance of lithium ion batteries? A sobering revelation from a completely nonflammable electrolyte. *Adv. Energy Mater.* **13**, 2203144 (2023).
23. Hou, J. et al. Thermal runaway of lihthium-ion batteries employing $LiN(SO_2F)_2$-based concentrated electrolyte. *Nat. Commun.* **11**, 5100 (2020).
24. Lee, S. et al. Interplay of cathode–halide solid electrolyte in enhancing thermal stability of charged cathode material in all-solid-state batteries. *ACS Energy Lett.* **9**, 1369–1380 (2024).
25. Choi, J. K. & Joncich, M. J. Heats of combustion, heats of formation and vapor pressures of some organic carbonates estimation of carbonate group contribution to heat of formation. *J. Chem. Eng. Data* **16**, 87–90 (1971).
26. Eshetu, G. G. et al. In-depth safety-focused analysis of solvents used in electrolytes for large scale lithium ion batteries. *Phys. Chem. Chem. Phys.* **15**, 9145–9155 (2013).
27. Heat of combustion of the elements. *Periodictable.com* https://periodictable.com/Properties/A/CombustionHeat.al.html (2024).
28. Pilcher, G., Pell, A. S. & Coleman, D. J. Measurements of heats of combustion by flame calorimetry part 2. Dimethyl ether, methyl ethyl ether, methyl *n*-propyl ether, methyl isopropyl ether. *Trans. Faraday Soc.* **60**, 499–505 (1964).
29. Heat of combustion for sulfolane. *Chemeo* https://www.chemeo.com/cid/98-351-4/Thiophene-tetrahydro-1-1-dioxide#ref-joback (2023).
30. Emmanuel, P. et al. An introduction to the combustion of carbon materials. *Chem. Eur. J.* **28**, e202200117 (2022).
31. Heat of combustion for $SOCl_2$. *Chemeo* https://www.chemeo.com/cid/63-179-4/Thionyl-chloride (2023).
32. Haynes, W. M. (ed.) *CRC Handbook of Chemistry and Physics* 92nd edn (CRC Press, 2011).

Acknowledgements
Partial financial support from Nissan Motor Co. Ltd and William E. Diefenderfer Endowment is gratefully acknowledged.

Author contributions
C.-Y.W., K.Q. and N.G. wrote the manuscript. S.G., N.G. and K.Q. designed and built the cells. S.G., K.Q., N.G. and T.S. carried out the experiments. C.-Y.W., K.Q., N.G., T.S. and K.A. participated in discussions and data interpretation. All authors contributed to the development of the manuscript as the project developed.

Competing interests
T.S. and K.A. are employed by Nissan Motor Co. Ltd. The other authors have no competing interests.

Additional information
Extended data is available for this paper at https://doi.org/10.1038/s41560-025-01887-6.

Supplementary information The online version contains supplementary material available at https://doi.org/10.1038/s41560-025-01887-6.

Correspondence and requests for materials should be addressed to Chao-Yang Wang.

Peer review information *Nature Energy* thanks Xiangming He and Atsuo Yamada for their contribution to the peer review of this work.

https://doi.org/10.1038/s41560-025-01887-6

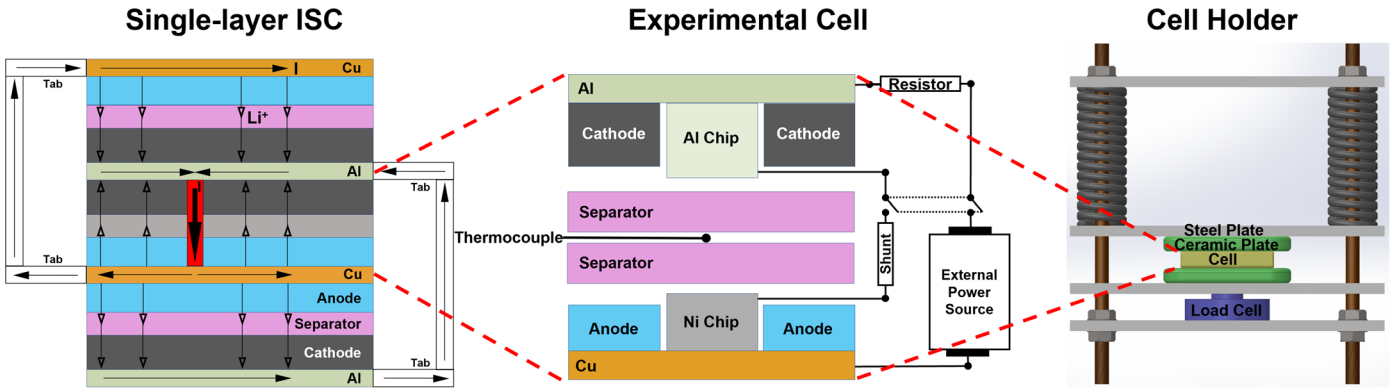

Extended Data Fig. 1 | Illustration of the physical problem and corresponding RISC experimental setup. Left, Single-layer internal short-circuit in a multilayer battery. Middle, Experimental cell in RISC method. Right, Cell holder with controllable stacking pressure. Figure adapted with permission from ref. 16, American Chemical Society.

https://doi.org/10.1038/s41560-025-01887-6

a

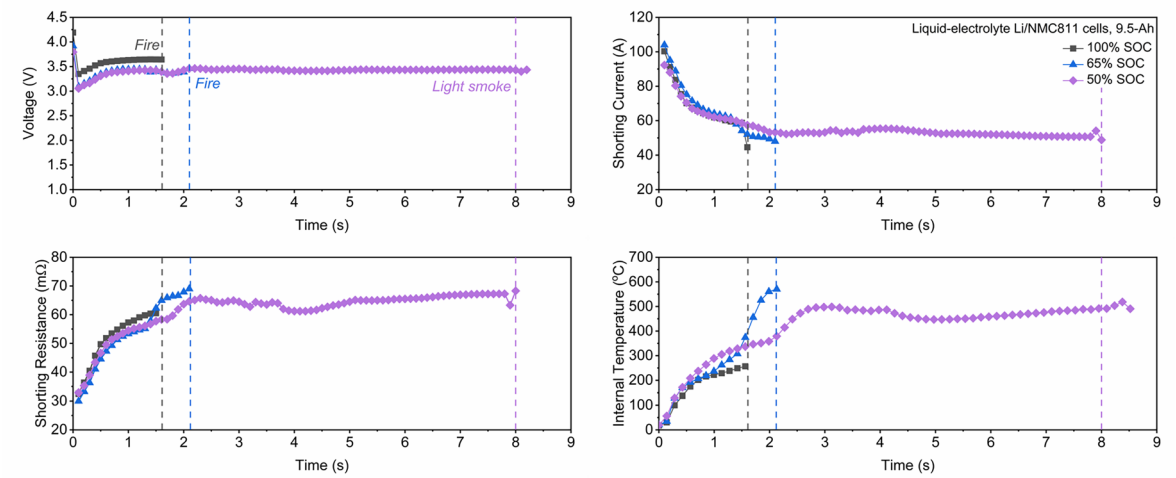

b

Extended Data Fig. 2 | Internal short circuiting of liquid-electrolyte graphite/NCM811 LiBs at various state of charge (SOC). a, Temporal variations of voltage, shorting current, shorting resistance and internal temperature at 100%, 65% and 50% SOC, respectively. **b**, Photographic images of LiB cells after ISC. The 100% and 65% SOC cells catch fires due to sufficient heat generated from electrolyte oxidation. In contrast, the 50% SOC cell, generating only half of reaction heat from electrolyte oxidation, emits light smokes only.